ChemPubSoc Europe

DOI: 10.1002/cptc.201900136

CHEMPHOTOCHEM Articles

Facile Two-Step Synthesis of Delafossite $CuFeO_2$ Photocathodes by Ultrasonic Spray Pyrolysis and Hybrid Microwave Annealing

Ivan Garcia-Torregrosa,[a] Yannick G. Geertzema,[a] Ahmed S. M. Ismail,[a] Tien-Lin Lee,[b] Frank M. F. de Groot,[a] and Bert M. Weckhuysen*[a]

Delafossite $CuFeO_2$ photocathodes have recently attracted attention for water splitting due to their suitable band gap (~ 1.5 eV) and high stability in aqueous media. The preparation of $CuFeO_2$ usually requires long and energy-intense treatments in an inert atmosphere for the full conversion of spinel $CuFe_2O_4$ to delafossite $CuFeO_2$. Herein, we report the preparation and characterization of highly uniform and stable $CuFeO_2$ thin films obtained via a combination of inexpensive ultrasonic spray pyrolysis followed by a short hybrid microwave treatment (~ 4 min). The resulting films show good stability in alkaline media and produce a photocurrent of ~650 μA/cm^2 under 1.5 AM simulated sunlight and with oxygen bubbling. The effect of the rapid transformation from the spinel to the delafossite phase induced by hybrid microwave annealing was investigated with synchrotron-based X-ray absorption spectroscopy (XAS) and X-ray photoelectron spectroscopy (XPS).

1. Introduction

With an ever-growing world population and an increasing demand for energy, clean and sustainable alternatives to fossil fuels are becoming an imminent necessity. Solar energy is one of the most promising sources of renewable energy, as there is a large excess of harvestable solar energy radiated onto the Earth's surface on a daily basis, and furthermore, the energy extraction process is generally completely carbon-free.[1] However, since solar radiation is variable over days and nights as well as over summers and winters, it is important to find an effective method for the intermittent storage of the renewable energy, so that it can be used at times when the radiation is less plentiful. This can be done by using chemical energy storage.

The bond in H_2 is very energy dense and therefore forms an excellent target for chemical energy storage. Photoelectrochemical water splitting is an elegant way to directly obtain hydrogen from water, and was first reported by Fujishima and Honda in 1975.[2] Nevertheless, a single semiconductor suitable for the evolution of H_2 and O_2 from H_2O using visible light and not suffering from severe degradation under the operating conditions hasn't yet been identified.[3] A currently attractive method for efficient solar energy harvesting and storage is through the use of the so-called D4 dual band gap system, whereby the photocathode and photoanode are stacked in tandem.[3,4] Photoanode materials have been relatively well defined in literature for the D4 system, with a lot of research focusing especially on hematite (α-Fe_2O_3), tungsten oxide (WO_3) and bismuth vanadate ($BiVO_4$).[5–9]

However, suitable photocathode materials stable in aqueous media remain more elusive, as most current options are either unstable at the working pH values of the D4 system or too expensive for implementation at a large scale.[4] $CuBi_2O_4$ photocathodes prepared by electrodeposition and sol-gel processing demonstrated decent photocurrents in neutral pH solutions.[10–13] More recently, $CuBi_2O_4$ photocathodes prepared by spray pyrolysis have been reported to outperform those prepared by the conventional sol-gel route when reducing H_2O_2.[14] Compared to $CuBi_2O_4$, delafossite $CuFeO_2$ has a number of characteristics that make it a promising contender as a photocathode material in a D4 system. The strong covalent nature of the Cu–O bonds, gives the delafossite material good hole mobility properties.[15] Delafossite photocathodes have also been reported to have high stabilities in high pH aqueous environments,[16] a prerequisite for any feasible photocathode material. Finally, and arguably also most importantly, $CuFeO_2$ has a band gap of around 1.55 eV which allows it to absorb a large portion of the solar spectrum, and its conduction band is positioned at −0.4 V, making it suitable for proton reduction and hydrogen generation under illumination.[17]

$CuFeO_2$ thin films have been previously synthesized using sophisticated methods such as pulsed laser deposition[18] and radio-frequency sputtering,[19] but these methods are unlikely to be implemented on a large scale as they are economically quite unfeasible. Recently, $CuFeO_2$ films have also been prepared using the simple sol-gel spin coating method showing high stability and good performance.[17,20,21] However, the films prepared in this manner require long processing steps

[a] I. Garcia-Torregrosa, Y. G. Geertzema, A. S. M. Ismail, Prof. Dr. F. M. F. de Groot, Prof. Dr. B. M. Weckhuysen
Utrecht University
Inorganic Chemistry and Catalysis Group
Universiteitsweg 99, 3584 CA Utrecht (The Netherlands)
E-mail: b.m.weckhuysen@uu.nl
[b] Dr. T.-L. Lee
Diamond Light Source Ltd.
Diamond Light Source
Didcot, Oxfordshire (United Kingdom)

Supporting information for this article is available on the WWW under https://doi.org/10.1002/cptc.201900136

and high temperature treatments under inert atmosphere leading to poor scalability. $CuFeO_2$ and mixtures of $CuFeO_2$ and CuO thin films were synthesized employing cathodic electrodeposition and their photoelectrochemical performance during HER and CO_2 reduction was demonstrated.[22–25] Nevertheless, the as-deposited films were amorphous and long heat treatments under Ar were necessary to obtain the desired delafossite phase. Spray pyrolysis was recently employed in the preparation $CuFeO_2$ thin films showing good film adhesion and crystallinity,[26–29] although no photoelectrochemical performance was yet reported. Ultrasonic spray pyrolysis (USP) was employed for the preparation of several photoanode and photocathode materials offering very conformal films with good crystallinity and improved performance,[30–32] being a fast and inexpensive deposition method.

In this work, we show that it is possible to form a mixed phase of spinel $CuFe_2O_4$ and delafossite $CuFeO_2$ with a Cu:Fe ratio close to unity through the use of ultrasonic spray pyrolysis (USP). In order to fully convert the film structure to delafossite, a short treatment of 3–4 min with hybrid microwave annealing (HMA) was employed. HMA offers the possibility of greatly reducing the heat treatment time while increasing the crystallinity of thin film semiconductors,[33,34] and it was demonstrated that a short HMA treatment could improve the photoelectrochemical performance of $CuFeO_2$ by 100% in just a few minutes.[35] More recently, HMA was employed for the fast synthesis of highly active $ZnFe_2O_4$ photoanodes with improved structural properties when compared to oven annealed counterparts.[36] This new synthesis method combining USP and HMA drastically reduces the time and energy cost for the preparation of homogeneous and photo-active $CuFeO_2$ photocathodes.

2. Results and Discussion

2.1. Characterization

One of the main difficulties of the ultrasonic spray pyrolysis (USP) preparation of multi-oxide films relates to obtaining the right precursors and stoichiometry of the elements in the bulk of the film, while keeping a dense and conformal coating. In this work a series of copper and iron precursors were explored resulting in very different morphologies. In addition, the solvent of choice must satisfy the requisites of good solubility, relatively low surface tension and high boiling point. Table S1 summarizes a list of solvents and precursors employed in the USP deposition. The substrates were heated at different temperatures from 350 °C to 475 °C obtaining the best results at 450 °C. In order to adjust the stoichiometry of the solutions employed during USP, inductively coupled plasma - optical emission spectroscopy (ICP-OES) was employed to estimate the final Cu/Fe composition of the films prepared at 450 °C, as shown by the plot of Figure S1 in supporting information. It is interesting to note that the ratio Cu/Fe in the final films was twice as much as the ratio Cu/Fe of the prepared solutions. Thermodynamically, the standard Gibbs free energy of formation in the range of temperatures studied, favors the Cu^+ state over the Cu^{2+} for copper oxides as reported by the Ellingham diagram of the CuO and Cu_2O formation (Figure S2).[39]

It could be expected that delafossite $CuFeO_2$ should form preferentially over spinel $CuFe_2O_4$ as the hot plate temperatures are increased. However, in our as-prepared samples, a mixed phase of spinel and delafossite can be observed in all the range of temperatures studied. The as-prepared films are therefore referred as $CuFeO_x$. Figure 1 shows the XRD patterns of a 35 USP cycles sample deposited on FTO glass as-prepared, after 2 h of heat treatment at 550 °C and after 3 min of HMA treatment. The as-prepared samples show some crystallinity with what seems to be a mixture of copper and iron oxides. The sample heat treated in air at 550 °C for 2 h shows increased crystallinity and a mixture of spinel and hematite patterns, while just after 3 min of HMA treatment the only phase present belongs to the rhombohedral ($R\bar{3}$m) delafossite $CuFeO_2$. We attribute the fast transformation from spinel to delafossite after the HMA treatment to two synergistic mechanisms. Firstly, the graphite used as susceptor inside the quartz vessel absorbs the majority of the microwave radiation reaching very high temperatures (≥750 °C) in a matter of seconds. That leads to a quick increase in temperature of the sample placed on top of the susceptor (for a more detailed description, see Figure S3) and depletion of the existing O_2 species in the sealed vessel as result of the combustion of graphite. Thus, a lower O_2 partial pressure atmosphere is created inside the vessel. Secondly, at the high temperature reached by the sample, microwave radiation starts coupling with the metal oxide thin-film depending on the dielectric loss factor, which increases exponentially with temperature.

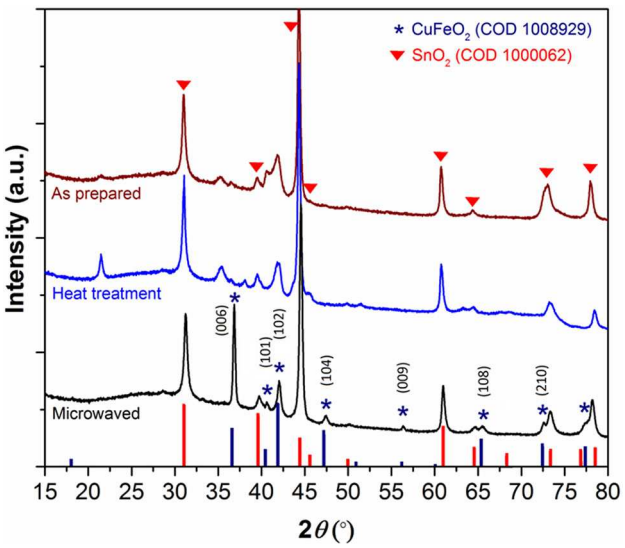

Figure 1. XRD patterns of a $CuFeO_x$ film deposited with 35 USP cycles as prepared (redline), heat treated at 550 °C for 2 h (blueline) and after HMA for 3 min (blackline). The X-ray source was CoKα (1.789 Å) and an integration time per step of 2s was employed.

As a result, in only 3 min of HMA treatment the bulk of the film is fully transformed into a reduced state. It is worth

mentioning that long HMA exposures, beyond 7 min, resulted in the deterioration of the thin-films, with Cu and Fe oxide peaks present in the subsequent cyclic voltammetries, as shown in Figure S4.

Though the crystal structure of the samples subjected to HMA treatment directly after USP deposition showed a full transformation to delafossite phase, the crystallinity of the samples heat treated at 550 °C for 2 h and then subjected to HMA was much higher. Employing the Scherrer equation [Eq. (1)], crystallite sizes of ~53 nm and ~103 nm were found for the samples microwave-treated after deposition and after annealing at 550 °C, respectively.

$$D = \frac{K \cdot \lambda}{\mathrm{FWHM} \cdot \cos\theta} \quad (1)$$

where λ is the X-ray wavelength in nm, while K is a constant related to the crystallite shape, FWHM is the peak width of the diffraction peak at half maximum height in radians.

SEM images of a 30 USP cycles photocathode after 550 °C and 3 min HMA are shown in Figure 2. The complete surface is free of pinholes or splashes with very conformal and macroporous morphology. From the inset of Figure 2a, it was estimated that the average grain size was 136 ± 12 nm. A FIB-SEM cross section of the sample (Figure 2b) shows the presence of macropores and good contact with the FTO substrate, while the revealed thickness was 283 ± 18 nm. Figure S5 shows that the as-prepared samples are dense and smoother, and only after the heat treatment for 2 h, the grain growth leads to a macroporous morphology. This grain growth phenomena reduces the final surface area, which might play a negative effect in the performance.

UV/Vis/NIR absorption spectra of the samples as-prepared (black line), heat-treated (red line) and HMA-treated (blue line) were obtained by subtracting the contribution of the FTO glass substrate, as shown in Figure 3b, where all three samples show

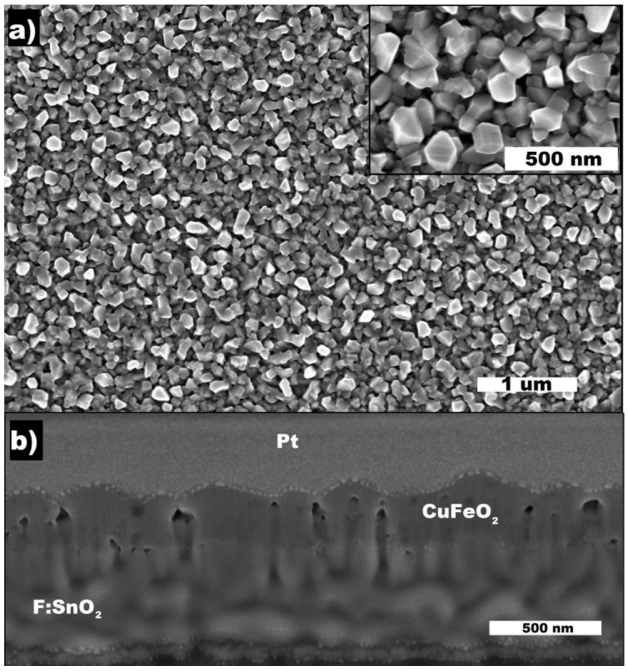

Figure 2. SEM images of a 30 UPS cycles sample on FTO glass after heat treatment at 550 °C and 3 min HMA treatment: a) top view and b) FIB-SEM section.

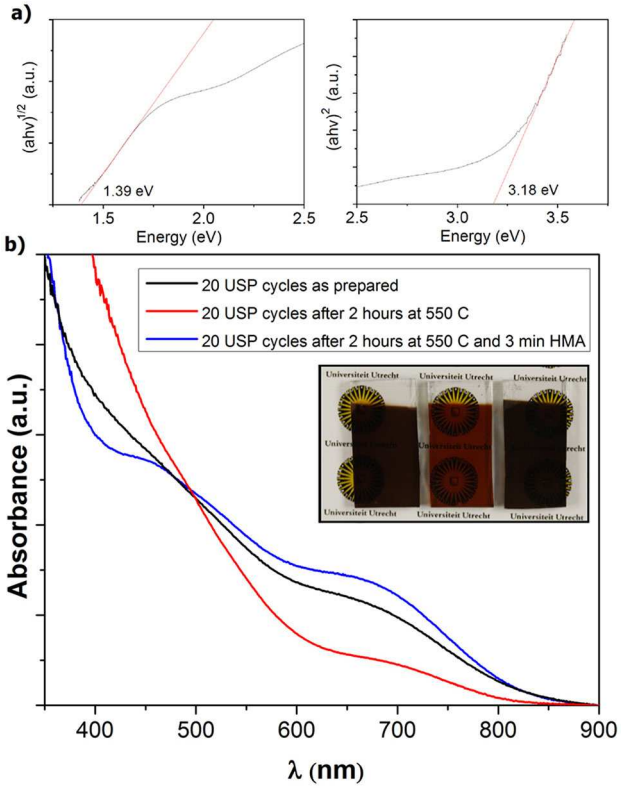

Figure 3. a) Direct (right) and indirect (left) Tauc plots of a 20 UPS cycles sample after microwave treatment for 3 min. b) UV-Vis-NIR spectra of a 20 USP cycles sample corrected for the substrate (FTO glass) as prepared (black line), heat treated for 2 h at 550 °C (red line) and microwaved for 3 min (blue line). Inset: Photograph of three samples, (left to right): as prepared, heat treated and microwaved for 3 min.

an onset around 900 nm. The optical properties of delafossite films were reported by Hiraga et al.[40] The (Cu 3d + O 2p) orbital contributes to the valence band and the (Cu $3d_z^2$ + 4 s) orbital to the conduction band, while the transition of (Cu 3d + O 2p)→(Cu $3d_z^2$ + 4 s) is responsible for the optical band gap of delafossite. Both the as-prepared and heat-treated films for 2 h show an absorption peak below the optical band gap assigned to the transition (Cu 3d + O 2p)→Fe t_{2g}, while the HMA-treated sample also shows the transition (Cu 3d + O 2p) Fe e_g. The Tauc plots of $(ahv)^n$ *vs.* *hv* presented in Figure 3a indicate that the films after HMA treatment show an indirect band gap of 1.39 eV (left) and a direct optical band gap of 3.18 eV (right). The inset of Figure 3b represents an optical image of a sample as-prepared (left), heat treated (middle) and after HMA treatment (right). Figure S6 shows the correlation between thickness and absorbance for a series of 10, 15, 20, 25 and 30 USP cycles

after heat treatment and HMA. There seems to be a linear correlation with the exception of the thickest sample.

To gain a further insight into the electronic properties of $CuFeO_2$ after preparation, heat treatment and brief microwave treatment, we employed complementary XAS and XPS measurements. Where 2p XAS probes the electronic excitation from 2p core states to empty 3d states yielding $2p^5\ 3d^{N+1}$ excitonic states, 2p XPS probes the excitations from 2p core states to free empty states, yielding a spectral shape dominated by screening due to the 3d states. The analysis of the Fe 2p edge XAS spectra in $CuFeO_2$ after preparation, heat treatment and microwave treatment showed that the main spectral features in the Fe 2p are similar for the sample after the three treatment conditions and is indicative of the presence of mostly Fe^{3+} ([Ar] 18 $4s^0$ $3d^5$]) in the system (Figure 4a).[41] However, the shoulder at ~708.3 eV seems to have higher intensity in the microwave treated sample than in the freshly prepared and the heat-treated sample. This observation may suggest the presence of small percentage of Fe^{2+} in the as-prepared and the heat-treated sample.[42] This small percentage of Fe^{2+} species were soon oxidized to Fe^{3+} upon microwave treatment to yield a Fe 2p XAS that shows pure Fe^{3+} state similar to the hematite reference spectra. This observation fits our expectation as it is expected that the sample after preparation and heat treatment would contain a spinel phase with mixed Fe^{3+}/Fe^{2+} that was rapidly transformed by short microwave treatment into the desired delafossite phase that contains solely Fe^{3+}. Additionally, the sharper features of Fe_2O_3 in the microwave treated sample reflect its better ordered crystal structure. It is worth noting that the Fe XAS in this sample is very similar to that of Fe_2O_3 as both Fe_2O_3 and $CuFeO_2$ contain Fe^{3+} in an octahedral symmetry.[43,44]

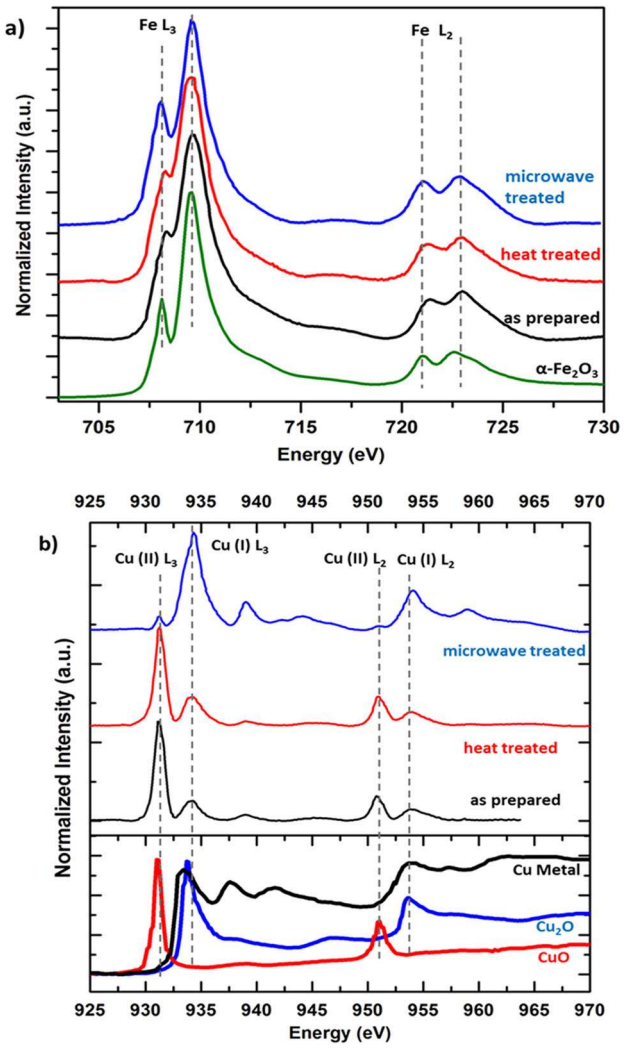

Figure 4. a) Fe 2p XAS and b) Cu 2p XAS profiles of $CuFeO_2$ after preparation, thermal treatment and microwave treatment; and their comparison with the XAS profiles of iron and copper references. The copper reference spectra have been adapted from Ref. [47].

On the other hand, the Cu 2p edge XAS showed that the oxidation state of Cu in the as-prepared and heat-treated samples is mainly Cu^{2+} ([Ar]18 $4s^0$ $3d^9$]) represented with an $2p_{3/2}$ and $2p_{1/2}$ edges at 931.5 eV and 953.5 eV, as observed in Figure 4b. The Cu spectra of the as-prepared and heat-treated samples also showed the presence of a smaller percentage of Cu^+ ([Ar]18 $4s^0$ $3d^{10}$]). Quantification of this Cu^+ amount from the XAS spectra showed that they represent around 36% of the Cu content in the as-prepared and heat-treated samples. However, the Cu 2p XAS of the microwave-treated sample showed that the Cu^+ percentage increased to around 90% of the sample's Cu content, which proves the effect of short microwave treatment on the $CuFeO_2$ spinel to delafossite phase transformation. Finally, since we recorded the XAS using TEY detection method, we estimated that the XAS probing depth of this experiment was ~2 nm, which probes the few $CuFeO_2$ layers below the surface.[45,46]

In addition, we have conducted XPS depth profiling at different excitation energies to probe the electronic properties of Fe, Cu, C and O at the surface (the top 0.5–1 nm) and compare this with their bulk electronic properties (at ~7.5–8 nm). The surface-sensitive XPS was conducted at an excitation energy of 1.15 KeV and showed that the Cu was always present as Cu^+ (recognizable by the doublet peaks at 932.6 eV and 952.4 eV) on the sample surface regardless of the type of treatment applied on the sample (Figure 5a). This observation is in agreement with the observation of Prévot et al.[21]

Interestingly, the more bulk-sensitive XPS that was conducted on the same spot on the sample with an excitation energy of 5.93 KeV (often referred to as HAXPES[42]), showed that Cu is present in the as-prepared and heat-treated samples as Cu^{2+} (recognizable by two satellite peaks of Cu $2p_{3/2}$ and Cu $2p_{5/2}$ at 942 eV and 961.7 eV, respectively), while it was reduced to mainly Cu^+ by the effect of brief microwave treatment (Figure 5b). The spectra of Fe 2p XPS (Figure 6) on the other hand, showed that Fe species remained mainly as Fe^{3+} in the surface and bulk irrespective of the sample treatment, which is in agreement with the observations from *refs.* [21] and [32].

Therefore, a combined XAS and XPS study was performed revealing that for the $CuFeO_2$ sample Fe was always present as Fe^{3+} in the surface and bulk of the sample, while Cu was present as mainly Cu^{2+} in the bulk and then was reduced to Cu^+ under the influence of microwave treatment, which

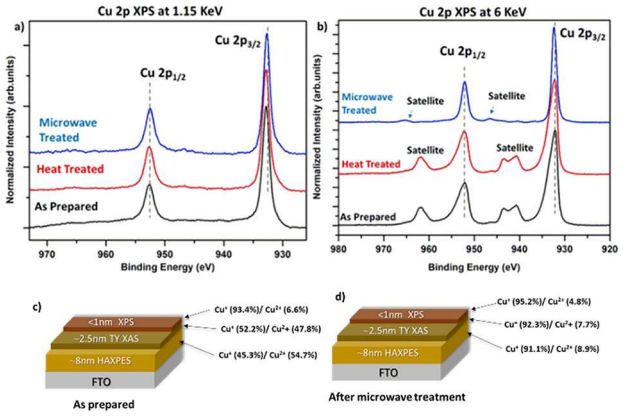

Figure 5. a) Cu 2p XPS spectra at 1.15 KeV excitation energy and b) Cu 2p XPS spectra at 5.93 KeV excitation energy in $CuFeO_2$ after preparation, thermal treatment and microwave treatment. c) Schematic of the elemental percentages of Cu^+ and Cu^{2+} in the as-prepared and d) microwave-treated samples at different probing depths.

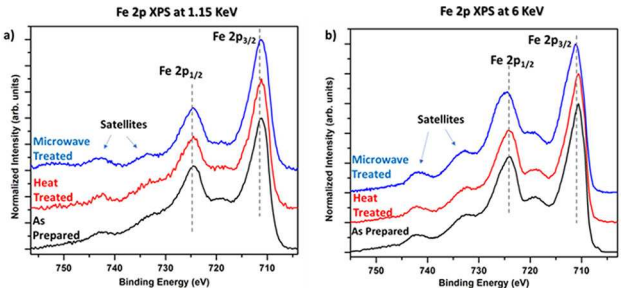

Figure 6. a) Fe 2p XPS spectra at 1.15 KeV excitation energy and b) Fe 2p XPS spectra at 5.93 KeV excitation energy in $CuFeO_2$ as-prepared, after thermal treatment and after microwave treatment.

confirms that a short microwave treatment of the sample transformed the CuO:Fe_2O_3 to the delafossite $CuFeO_2$ phase. On the sample's surface, Cu was permanently present as Cu^+ irrespective of the sample treatment procedures.

Finally, C 1s XPS investigation showed that C was present extensively on the sample's surface after microwave treatment in comparison with its presence in the as-prepared and heat-treated sample, as observed in Figure 7. Nevertheless, its concentration did not show a significant change in the bulk after microwave treatment. This finding may give an important

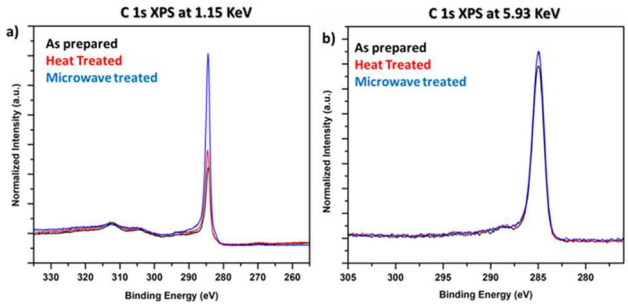

Figure 7. a) C 1s XPS spectra at 1.15 KeV and b) at 5.93 KeV excitation energy in $CuFeO_2$ after preparation, thermal treatment and microwave treatment.

indication on the stability of surface Cu^+ as it is possible that some sort of a relatively carbon-rich phase is formed at the surface (carbide or carbonyl) during microwave treatment that may have an effect on the Cu oxidation state as well as in the photoelectrochemical activity of $CuFeO_2$ photocathodes.

2.2. Photoelectrochemical Performance

In order to characterize the photoelectrochemical activity and stability of the resulting photocathodes, they were placed in a home-made PEC cell fitted with an optical grade quartz window and filled with 140 mL of a 1 M NaOH solution. A Pt coil was employed as the counter electrode and a saturated Ag/AgCl as reference electrode. It was reported that $CuFeO_2$ delafossite photocathodes prepared by sol-gel and annealed in Ar at 700 °C, show negligible activities towards the hydrogen evolution reaction (HER).[16,17] Our results are in agreement with the reported values, as shown in the sweep voltammetries in Figure 8. Where a 30 USP cycles photocathode was intermit-

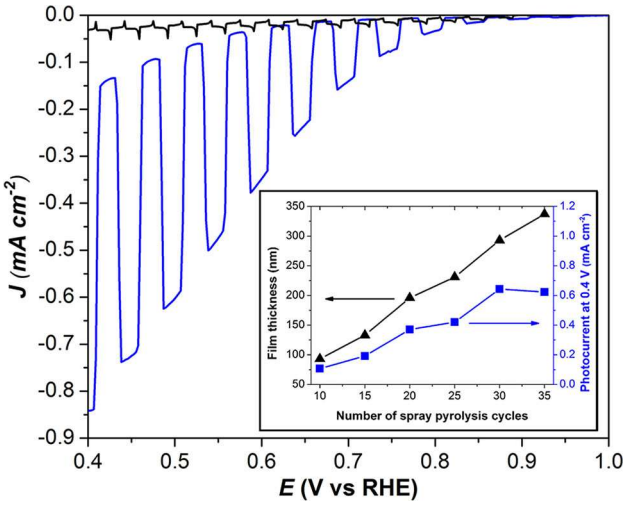

Figure 8. Chopped light linear sweep voltammetry in the cathodic direction of a 30 USP cycles photoelectrode after heat treatment for 2 h and HMA for 3 min, in a 1 M NaOH solution saturated with O_2 (blue line) and saturated with Ar (black line). The scan rate was 10 mV/s and the sample was illuminated from the front. The inset represents the relation between the number of USP cycles versus the film thickness and photocurrent at 0.4 V vs. RHE.

tently illuminated from the front (electrolyte/film junction) in an O_2-saturated solution (blue line) and an Ar-saturated solution (black line). Clearly, in the absence of a sacrificial agent low photocurrents in the order of 10 μA/cm^2 indicate that there is no evolution of H_2. A maximum photocurrent of about ~650 μA/cm^2 was found for a 30 USP cycles or around 300 nm thick sample at 0.4 V vs. RHE. The inset in Figure 8 shows the correlation of the thickness and number of USP cycles with the observed photocurrents. The photocurrent values increase almost linearly with the film thickness up to 300 nm, where the optimum performance is achieved, while thicknesses beyond 300 nm seem to start showing a detrimental effect in the

performance. A similar optimal film thickness was reported by Prevot et al., where it was concluded that the poor charge separation of the films was the main limitation for the photoactivity of thicker samples.[17]

Compared to the reported sol-gel synthesized samples in the literature, where long duration heat treatments are carried out after each spin coated/dip coated layer, our $CuFeO_2$ delafossite samples were prepared in less than three hours combining USP (~30 min), heat treatment (~2 h) and HMA (3–4 min) showing good activity towards O_2 reduction. In addition, it is worth noting that contrary to the conventional fabrication methods where a final annealing step under inert atmosphere is necessary to achieve the $CuFeO_2$ delafossite phase,[16–20] no further annealing treatment was employed in our combined USP and HMA synthesis procedure. However, XPS measurements revealed that a higher amount of C was detected at the surface of the films after the HMA treatment, which might cause a loss of active surface area. Further investigations on the surface chemistry should be addressed in order to enhance the activity towards HER.

The stability of the samples was studied with chronoamperometry under strong O_2 bubbling and on/off cycles of 55 s each. Figure 9 shows the stability of a 30 USP cycles photocathode polarized at 0.4 V vs. RHE during 6000 s without noticeable change except for the first 20 min of the experiment where a clear decrease in dark current from ~370 μA/cm^2 to about ~140 μA/cm^2 takes place. The reason for this change in dark current is not yet clear and a similar trend happens in all the investigated films regardless their thickness. In order to assess any possible structural changes, samples subjected to polarization were investigated with UV-Vis-NIR spectroscopy and XRD before and after the polarization experiment showing no major changes in absorbance or crystal structure. We note that the resulting data in the chopped light chronoamperometric scan shows excessive noise due to the intense oxygen bubbling in the electrolyte solution during the experiment.

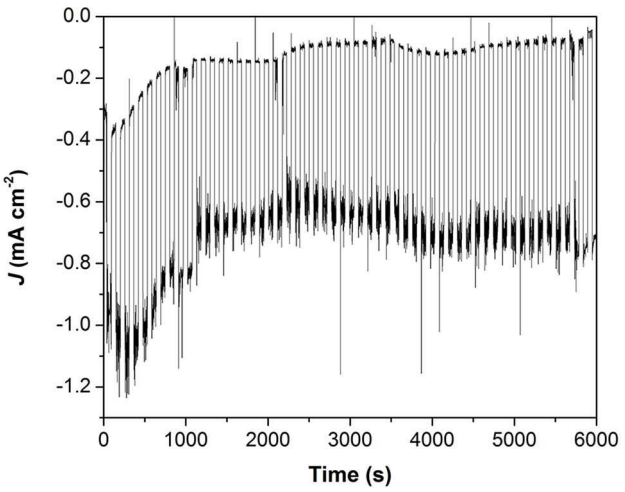

Figure 9. Chronoamperometry of a bare 30 USP cycles $CuFeO_2$ photocathode at 0.4 V vs. RHE in a 1 M NaOH solution with strong O_2 bubbling under chopped 1.5 AM simulated illumination.

3. Conclusions

A fast and scalable method for the synthesis of conformal and stable $CuFeO_2$ photocathodes combining a solution-based ultrasonic spray pyrolysis process (USP) followed by a short hybrid microwave annealing treatment (HMA) was demonstrated. The resulting samples show a photocurrent of 650 μA/cm^2 under one sun illumination and O_2 as sacrificial agent without any further surface treatment. XRD and UV-Vis-NIR spectroscopy show a complete transformation from spinel $CuFe_2O_4$ to delafossite $CuFeO_2$ after three min of HMA treatment, while XAS indicate a major presence of Cu^+ and Fe^{3+} in the bulk and the surface of $CuFeO_2$. XPS indicates the enrichment of carbonaceous species at the surface. Further surface investigations are necessary to conclude the effect of such carbon-rich species and improve the selectivity towards proton reduction. In combination with active and inexpensive co-catalysts, such as Ni–Mo or Ni–Mo–S, the proposed synthesis for $CuFeO_2$ shows promise for its use as photocathode in a D4 tandem system.

Experimental Section

Materials

$Fe(C_5H_7O_2)_3$ (Acros Organics, 99% pure), $Cu(NO_3)_2 \cdot 3H_2O$ (Acros Organics, 99% pure), Dimethylformamide (DMF, Fisher Scientific, 99% pure) were used for the direct deposition of $CuFeO_x$ by ultrasonic spray pyrolysis. NaOH (Emsure, 99%) was used as pH buffer in the photoelectrochemical cell. The films were deposited on F:SnO_2 (FTO) coated glass (Pilkington, TEC15).

Substrate Preparation

FTO coated glass (Pilkington, TEC 15) was cut in 3×1.5 cm pieces. Both sides were mechanically cleaned with CIF detergent twice and sonicated in 1:1:1 demiwater:ethanol:acetone for 15 min in an ultrasound bath at 45 KHz and 100 W. Afterwards the solution was changed for 1 M HCl followed by another 15 min ultrasound. The pieces were rinsed with demi-H_2O after each step and were stored in demi-H_2O. Before the reaction the fragments were dried with N_2 and placed in UV/O_3 procleaner (Bioforce) for 15 min.

Spray Pyrolysis Deposition

In a typical experiment, Fe(acac) (Acros Organics, 99% pure, 50 mM) and $Cu(NO_3)_2 \cdot 3H_2O$ Acros Organics, 99% pure, 25 mM) were dissolved in DMF (Fisher Scientific, 99% pure) and stirred overnight. The resulting solution was deposited using ultrasonic-spray pyrolysis on cleaned FTO substrate at different temperatures from 350 °C to 450 °C. For the atomization of the solution, a Sonaer 60 kHz narrow nozzle spray equipped with a wide vortex was employed, fixing the power from 1.8 W to 2.2 W. The precursor solution was dispensed through a single micro-feed channel with a flow rate of 2 mL/min, and compressed N_2 with a flux of 2 L/min was employed as carrier gas. One spray pyrolysis cycle consisted of 20 s spray pyrolysis, 45 s pause, 20 s spray pyrolysis, 45 s pause, providing an average of ~10 nm film growth per spray pyrolysis cycle. After deposition, the films were slowly cooled down to room temperature to prevent the substrate from cracking.

Heat Treatment

In order to improve the homogeneity and crystallinity of the thin films, a heat treatment was performed. The samples were placed in a muffle oven and heated to 550 °C with a ramp of 5 °C/min and kept at that temperature for 2 h.

Hybrid Microwave Annealing

After deposition, the films were placed in a quartz beaker filled with 8 g of graphite powder. The graphite was partially compressed in the central area where the sample was placed and uncompressed near the border of the setup, (see Figure S3). The quartz beaker was closed using a ceramic lid and placed in a commercial microwave (Sharp 2.4 GHz 800 W) and microwaved from 3 to 7 min.

Characterization of Films

The electronic transitions and band gaps of the materials were studied using a UV-VIS-NIR spectrometer. Both transmittance and absorption spectra were recorded from 900 nm to 350 nm making use of a UV-vis-NIR Cary 500 (Varian) spectrophotometer. Using a D2 (Bruker) diffractometer, equipped with a Co Kα X-ray source excited at 30 kV and 10 mA, the X-ray diffraction (XRD) patterns were acquired from 20° to 80° 2θ angles. The acquisition conditions for the diffractograms were 0.04° step size and 2 s integration time. Scanning electron microscopy (SEM), using of a FEI Helios Nanolab 600 FIB-SEM instrument at 5 kV acceleration voltage, was used to acquire detailed information of the surface and thickness of the material. X-ray absorption spectroscopy (XAS) and X-ray photoelectron spectroscopy (XPS) experiments were performed at the Surface and Interface Structural Analysis beamline (I09) at the Diamond Light Source (UK). During the XAS experiments, the monochromator was scanned across the Fe 2p absorption edge (700–740 eV) and Cu 2p absorption edge (920–980 eV). The energy resolution of the recorded spectra was 100 meV and the measurements were taken in total electron yield (TEY) mode where the X-ray probing depth was estimated to be around 2 nm. For the Cu species quantification from XAS, we normalized the spectra to the rising absorption edge. The Fe and Cu XPS measurements were recorded using two different excitation energies; 1.15 KeV and 5.93 KeV with an energy resolution of 100 meV. Since the I09 end station provides the possibility to focus two X-ray beams at the same spot on the sample, we were able to conduct XPS depth profiling on the Fe and Cu in each sample in the same chamber directly after each other and without having to use Ar sputtering to etch the sample surface, which was shown to affect the electronic properties of elements in previous studies.[37,38]

As the binding energy (E_b) of the core level electrons is constant, the kinetic energy (E_k) increases with increasing the photon energy ($\hbar\omega$). This relation is described by the Einstein's photoelectric effect equation ($Ek = \hbar\omega - Eb - \Phi$) where Φ is the spectrometer work function. By increasing the kinetic energy, the electron mean free path in the sample increases, hence getting information from a larger depth in the sample and reducing surface state effect (such as the adsorption of carbon and hydroxyl groups). The calculated electron inelastic mean free path (IMFP) at 1.15 KeV excitation energy ranged from 0.5 nm for Cu and 1 nm for Fe, respectively. On the other hand, the electron IMFP at 5.9 KeV was 7.2 nm for Cu and 7.4 for Fe, respectively. The 100 μm X-ray beam was set at 20° take-off angle with respect to the sample surface. The pass energy was 50 eV at 1.15 KeV excitation energy and 200 eV and 5.93 KeV excitation energy. The XPS spectral background was subtracted using the Shirley method in the CASA XPS software. Three $CuFeO_2$ samples were investigated: As prepared, after heat treatment for 2 h and after microwave treatment for 3 min.

Photoelectrochemical Measurements

Photoelectrochemical (PEC) measurements were performed using a potentiostat (Autolab PGSTAT204 compact potentiostat) using a three-electrode cell with CuFeO2, saturated Ag/AgCl and Pt coil as working, reference and counter electrodes respectively. The electrolyte was comprised of 1 M NaOH. The PEC cell was illuminated using a 75 W Xe arc lamp with a 1.5 AM filter calibrated to 100 mW/cm^2. All the samples were masked leaving 0.27 cm^2 exposed to the electrolyte.

Acknowledgements

We acknowledge financial support from Netherlands Centre for Multiscale Catalytic Energy Conversion (MCEC) as well as the Netherlands Organization for Scientific Research (NWO). Additional support came from a Strategic Alliance program between Utrecht University and Eindhoven University of Technology.

Conflict of Interest

The authors declare no conflict of interest.

Keywords: artificial photosynthesis · $CuFeO_2$ photocathodes · photoelectrochemistry · water splitting · X-ray absorption spectroscopy

[1] M. Graetzel, *Nature* **2001**, *414*, 338–344.
[2] A Fujishima, K. Kohayakawa, K. Honda, *J. Electrochem. Soc.* **1975**, *122*, 1487–1489.
[3] M. S. Prevot, K. Sivula, *J. Phys. Chem. C* **2013**, *117*, 17879–17893.
[4] K. Sivula, M. Graetzel. Photoelectrochemical Water Splitting: Materials, Processes and Architectures (pp 83–105) London: RSC Publishing.
[5] K. Sivula, F. Le Formal, M. Graetzel, *ChemSusChem* **2011**, *4*, 432–449.
[6] A. J. Abel, I. Garcia-Torregrosa, A. M. Patel, B. Opasanont, J. B. Baxter, *J. Phys. Chem. C*, **2015**, *119*, 4454–4465.
[7] B. D. Alexander, P. J. Kulesza, I. Rutkowska, R. Solarska, J. Augustynski, *J. Mater. Chem.* **2008**, *18*, 2298–2303.
[8] F. F. Abdi, L. Han, A. H. M. Smets, M. Zeman, B. Dam, R. van de Krol, *Nat. Commun.* **2013**, *4*, 2195.
[9] Y. Park, K. J. McDonald, K. S. Choi, *Chem. Soc. Rev.* **2013**, *42*, 2321–2337.
[10] D. Kang, J. C. Hill, Y. Park, K. Choi, *Chem. Mater.*r. **2016**, *28*, 4331–4340.
[11] H. S. Park, C. Lee, E. Reisner, *Phys. Chem. Chem. Phys.* **2014**, *16*, 22462–22465.
[12] D. Cao, N. Nasori, Z. Wang, Y. Mi, L. Wen, Y. Yang, S. Qu, Z. Wang, Y. Lei, *J. Mater. Chem. A* **2016**, *4*, 8995.
[13] S. P. Berglund, F. F. Abdi, P. Bogdanoff, A. Chemseddine, D. Friedrich, R. van de Krol, *Chem. Mater.* **2016**, *28*, 4231–4242.
[14] F. Wang, A. Chemseddine, F. F. Abdi, R. van de Krol, S. P. Berglund, *J. Mater. Chem. A* **2017**, *5*, 12838.
[15] H. Kawazoe, H. Yanagi, K. Ueda, H. Hosono, *MRS Bull.* **2000**, *25*, 28–36.
[16] C. G. Read, Y. Park, K. S. Choi, *J. Phys. Chem. Lett.* **2012**, *3*, 1872–1876.
[17] M. S. Prevot, N. Guijarro, K. Sivula, *ChemSusChem* **2015**, *8*,1359-1367.
[18] S. Z. Li, J. Liu, X. Z. Wang, B. W. Yan, H. Li, J. M. Liu, *Phys. B Condens. Matter* **2012**, *407*, 2412–2415.
[19] A. Barnabe, E. Mugnier, L. Presmanes, P. Tailhades, *Mater. Lett.* **2006**, *60*, 3468–3470.
[20] H. Chen, J. Wu, *Thin Solid Films* **2012**, *520*, 5029–5035.

[21] M. S. Prevot, X. A. Jeanbourquin, W. S. Bouree, F. Abdi, D. Friedrich, R. van de Krol, N. Guijarro, F. Le Formal, K. Sivula, *Chem. Mater.* **2017**, *29*, 4952–4962.
[22] C. G. Read, Y. Park, K. Choi, *J. Phys. Chem. Lett.* **2012**, *3*, 1872–1876.
[23] G. Riveros, C. Garí, D. Ramírez, E. A. Dalchiele, R. E. Marotti, C. J. Pereyra, E. Spera, H. Gómez, P. Grez, F. Martín, J. R. Ramos-Barrado, *Electrochim. Acta* **2015**, *164*, 297–306.
[24] U. Kang, S. K. Choi, D. J. Ham, S. M. Ji, W. Choi, D. S. Han, A. Abdel-Wahab, H. Park, *Energy Environ. Sci.* **2015**, *8*, 2638–2643.
[25] U. Kang, H. Park, *J. Mater. Chem. A* **2017**, *5*, 2123–2131.
[26] A. H. O. Alkhayatt, S. A. Thahab, I. A. Zgair, *Optik* **2016**, *127*, 3745-3749.
[27] P. Pizá-Ruiz, A. Sáenz-Trevizo, Y. Verde-Gómez, P. Amézaga-Madrid, M. Miki-Yoshida, *Ceram. Int.* **2019**, *45*,1156-1162.
[28] H. M. Abdelwahab, A. Ratep, A. M. Abo Elsoud, M. Boshta, M. B. S. Osman, *Results Phys.* **2018**, *9*, 1112–1115.
[29] A. Duret, M. Graetzel, *J. Phys. Chem. B* **2005**, *109*, 17184–17191.
[30] M. Li, L. Zhao, L. Guo, *Int. J. Hydrog. Energy* **2010**, *35*, 7127–7133.
[31] S. Huang, W. Luo, Z. Zou, *J. Phys. D* **2013**, *46*, 235108.
[32] A. Ginsburg, D. A. Keller, H. Barad, K. Rietwyk, Y. Bouhadana, A. Anderson, A. Zaban, *Thin Solid Films* **2016**, *615*, 261–264.
[33] J. Y. Kim, D. H. Youn, J. H. Kim, H. G. Kim, J. S. Lee, *ACS Appl. Mater. Interfaces* **2015**, *7*, 14123–14129.
[34] J. H. Kim, Y. H. Jo, J. H. Kim, J. S. Lee, *Nanoscale* **2016**, *8*, 17623.
[35] Y. J. Jang, Y. B. Park, H. E. Kim, Y. H. Choi, S. H. Choi, J. S. Lee, *Chem. Mater.* **2016**, *28*, 6054–6061.
[36] J. H. Kim, Y. J. Jang, S. H. Choi, B. J. Lee, M. H. Lee, J. S. Lee, *ACS Sustainable Chem. Eng.* **2019**, *7*, 944–949.
[37] E. Lewin, P. O. A. Persson, M. Lattermann, M. Stüber, M Gorgoi, A. Sandell, C. Ziebert, F. Schäfers, W. Braun, J. Halbritter, S. Ulrich, W. Eberhardt, H. Siegbahn, S. Svensson, U. Jansson, *Surf. Coat. Technol.* **2008**, *202*, 3563–3570.
[38] M. Fondell, M. Gorgoi, M. Boman, A. Lindblad, *J. Electron Spectrosc. Relat. Phenom.* **2018**, *224*, 23–26.
[39] M. J. Balart, J. B. Patel, F. Gao, Z. Fan, *Metall. Mater. Trans.* **2016**, *47*, 4988–5011.
[40] H. Hiraga, T. Makino, T. Fukumura, H. Weng, M. Kawasaki, *Phys. Rev. B* **2011**, *84*, 041411.
[41] P. S. Miedema, F. M. F. de Groot, *J. Electron Spectrosc. Relat. Phenom.* **2013**, *187*, 32–48.
[42] B. Zhang, X. Zhen, O. Voznyy, R. Comin, M. Bajdich, M. García-Melcho, L. Han, *Science* **2016**, *352*, 333–337
[43] V. Galakhov, A. Poteryaev, E. Kurmaev, V. Anisimov, S. Bartkowski, M. Neumann, *Condens. Matter Phys.* **1997**, *56*, 4584–4591.
[44] R. Grau-Crespo, A. Y. Al-Baitai, I. Saadoune, N. H. de Leeuw, *J. Phys. Condens. Matter* **2010**, *22*, 25.
[45] M. Abbate, J. B. Goedkoop, F. M. F. de Groot, M. Grioni, J. C. Fuggle, S. Hofmann, H. Petersen, M. Sacchi, *Surf. Interface Anal.* **1992**, *18*, 65–69.
[46] J. J. Mudd, T. Lee, V. Muñoz-Sanjosé, J. Zuniga-Perez, D. Hesp, J. M. Kahk, D. J Payne, R. G. Egdell, C. F. McConville, *Phys. Rev. B* **2014**, *89*, 035203.
[47] M. Grioni, J. B. Goedkoop, R. Schoorl, F. M. F de Groot, J. C. Fuggle, F. Schafers, E. E. Koch, G. Rossi, J. M. Esteva, R. C. Karnatak, *Phys. Rev. B* **1989**, *39*, 1541–1545.

Manuscript received: May 4, 2019
Revised manuscript received: July 28, 2019
Accepted manuscript online: August 2, 2019
Version of record online: September 10, 2019